# Solidification around a cylinder in laminar cross flow

**H. Chiang and C. Kleinstreuer**
Department of Mechanical and Aerospace Engineering, North Carolina State University, Raleigh, NC, USA

Liquid–solid phase change problems in convection heat transfer have many engineering applications. The Navier–Stokes and energy equations have been solved for transient laminar two-dimensional flow past a horizontal subcooled cylinder with outward solidification. The irregular, moving solid–liquid regions have been transformed into uniform squares for easier numerical problem solution using an ADI finite difference scheme. Results discussed are the unsteady thermal flow patterns, solid–liquid interface locations, Nusselt number distributions, and rates of ice formation for different Reynolds numbers, superheat parameters and Stefan numbers. After the initial phase of conduction-controlled ice layer growth, forced convection heat transfer may strongly affect the freezing process, potentially causing irregular shapes of ice formation.

**Keywords:** phase change; horizontal cylinder; cross flow; moving boundary problem; Navier–Stokes equations

## Introduction

Liquid–solid phase change problems with moving boundaries have numerous applications. Examples include: ice cover formation, metal casting, crystal growing, frost layer formation, food stuff freezing, heat shield ablation, ice melting, latent heat storage, and soil freezing or thawing. One common characteristic of these Stefan-like problems is that phase change and an associated source or sink of latent heat occurs at the (unknown) moving interface. Furthermore, conductive heat fluxes governed by the Stefan number (i.e., ratio of sensible heat to latent heat), and the property value ratios of the phase change material are important in all of these processes. However, subcooling of the solid, possible density abnormalities of the liquid, and natural convection may be dominant in melting processes[1,2] whereas outward solidification in a liquid stream past a cooled wall may be more determined by mechanisms of forced convection heat transfer and/or by the characteristics of the superheated fluid.[3,4] Hirata *et al.*[3] measured steady-state ice layer profiles on an isothermal horizontal plate in a free stream and extended the analysis theoretically using a modified Reynolds number as the correlation parameter. Lock and Kaiser[4] studied ice formation on single vertical tubes and the generation of an ice vail around twin tubes in a river. Their theoretical analysis, assuming steady growth of concentric ice layers, was supported by experiments in a water tunnel with single and twin cylinders. In related studies, Karniadakis[5] used a commercial code based on the spectral element method to solve the unsteady Navier–Stokes and energy equations for laminar two-dimensional flow past a heated cylinder. The emphasis was on the structure of the near wake for Reynolds numbers up to 200 and the Nusselt number distributions for different thermal boundary conditions. Lunardini[6] analyzed freezing and thawing of concentric regions around a cylinder assuming transient thermal diffusion only. Based on a rather simple numerical solution employing the heat balance integral method, phase change locations and surface heat transfer rates are discussed for different system parameters. Solomon *et al.*[7] replaced the transient conduction heat transfer equation for the Stefan problem with the telegrapher's equation. They argued that Fourier's law should be more realistically replaced by $\vec{q}(\vec{x}, t+\hat{\tau}) = -k\nabla T$, where $\hat{\tau}$ is called the response or relaxation time of the phase change material. Additional references are given in subsequent sections.

Concentrating on the freezing process of water at low Stefan numbers around a cylinder in cross flow, the complete transport equations for laminar two-dimensional flow are transformed and solved numerically using an ADI finite difference scheme.[8] It is of interest to analyze forced convection heat transfer along the moving interface and to compute the growth rate of solidifying material for different system parameters. Because of the lack of experimental data sets for the complete system, our predictive results from special case studies are compared with measurements of single-phase as well as two-phase conduction dominated and convection controlled heat transfer processes.

## Analysis

Consider a cylinder of diameter $D$ in uniform cross flow of a phase-change material with temperature $T_0$. The cylinder temperature is suddenly lowered below the fusion temperature of the liquid, i.e., $T_w < T_f = 0°C$, and a solid layer is formed around the cylinder, changing the immediate velocity field. While the cylinder surface remains at the constant temperature $T_w$, the local velocity field and temperature distributions in the solid and liquid are changing with time $t$, coupled via the unknown interface location $R = R(\theta, t)$ which stays at $T = T_f$. Figure 1 depicts the problem of interest and the coordinate system used. Assuming two-dimensional laminar flow of Newtonian fluids with constant properties, the differences in volume associated with phase change are neglected as well as cylinder end effects, natural convection, and vortex shedding.

Employing the stream-function/vorticity approach, the tran-

Address reprint requests to Dr. Kleinstreuer at the Department of Mechanical and Aerospace Engineering, North Carolina State University, Raleigh, NC 27695-7910, USA.

Received 5 July 1988; accepted 28 March 1989

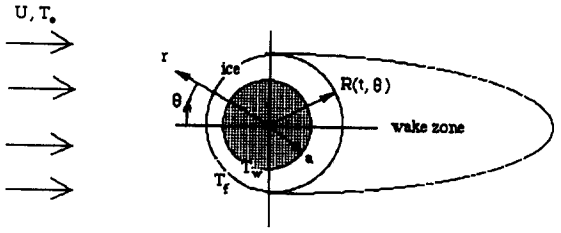


*Figure 1* Schematics for outward solidification around a subcooled cylinder

sient Navier–Stokes equations for two-dimensional flow in polar coordinates are written as

$$\frac{\partial\tilde{\omega}}{\partial t}+\frac{1}{r}\left[\frac{\partial}{\partial\theta}\left(\tilde{\omega}\frac{\partial\tilde{\psi}}{\partial r}\right)-\frac{\partial}{\partial r}\left(\tilde{\omega}\frac{\partial\tilde{\psi}}{\partial\theta}\right)\right]=\nu\nabla^2\tilde{\omega} \tag{1}$$

and

$$\tilde{\nabla}^2\tilde{\psi}=-\tilde{\omega} \tag{2}$$

where

$$\frac{\partial\tilde{\psi}}{\partial\theta}=-r\tilde{v},\quad \frac{\partial\tilde{\psi}}{\partial r}=\tilde{u},\quad \tilde{\nabla}^2=\frac{\partial^2}{\partial r^2}+\frac{1}{r}\frac{\partial}{\partial r}+\frac{1}{r^2}\frac{\partial^2}{\partial\theta^2}\text{ and} \tag{3a–d}$$

$$\tilde{\omega}=\frac{1}{r}\left[\frac{\partial}{\partial r}(r\tilde{v})-\frac{\partial\tilde{u}}{\partial\theta}\right]$$

The associated boundary conditions are for $t\geq 0$:

$$\tilde{\omega}=\tilde{\psi}=0 \quad \text{at } \theta=0 \text{ and } \pi \quad \text{(symmetry)} \tag{4a}$$

$$\tilde{\psi}=\frac{\partial\tilde{\psi}}{\partial r}=0 \quad \text{for } r=R(\theta,t) \quad \text{(no slip)} \tag{4b,c}$$

and

$$\tilde{\psi}=-rU\sin\theta \quad \text{and} \quad \tilde{\omega}=0 \quad \text{as } r\to\infty \quad \text{(potential flow)} \tag{4d,e}$$

The temperature field in the liquid phase is described by the transient convection–conduction equation.

$$\frac{\partial\tilde{T}}{\partial t}+\frac{1}{r}\left[\frac{\partial}{\partial\theta}\left(\tilde{T}\frac{\partial\tilde{\psi}}{\partial r}\right)-\frac{\partial}{\partial r}\left(\tilde{T}\frac{\partial\tilde{\psi}}{\partial\theta}\right)\right]=\alpha_l\tilde{\nabla}^2\tilde{T} \tag{5}$$

$$\text{At } t<t_0, \quad \tilde{T}=\tilde{T}_0 \text{ and for } t\geq t_0,\ \tilde{T}=\tilde{T}_f \text{ at } r=R(\theta,t) \tag{6a,b}$$

$$\text{As } r\to\infty, \quad \tilde{T}=\tilde{T}_0 \text{ and } \frac{\partial\tilde{T}}{\partial\theta}=0 \text{ at } \theta=0 \text{ and } \pi \tag{6c,d}$$

Equation 5 can be reduced for the solid region to

$$\frac{\partial\tilde{T}}{\partial t}=\alpha_s\tilde{\nabla}^2\tilde{T} \tag{7}$$

subject to

$$\tilde{T}=\tilde{T}_f \text{ at } r=R(\theta,t) \text{ and } \tilde{T}=\tilde{T}_w \text{ for } r=a \tag{8a,b}$$

Symmetry requires that

$$\frac{\partial\tilde{T}}{\partial\theta}=0 \quad \text{at } \theta=0 \text{ and } \pi \tag{8c}$$

A heat balance at the solid–liquid interface $R(\theta,t)$ yields

$$\rho_s L\frac{dR}{dt}=\left[1+\left(\frac{1}{R}\frac{\partial R}{\partial\theta}\right)^2\right]\left(k_s\frac{d\tilde{T}}{dr}-k_l\frac{d\tilde{T}}{dr}\right) \tag{9}$$

In order to facilitate the numerical work, the irregular solidification front in the physical domain is transformed to a rectangular shape in the computational domain using body-fitted coordinates. Considering first the *liquid* region, a fine grid is required near the interface with a smooth transition to a coarse grid for the outer region. Hence an exponential function for the $r$-coordinate is postulated, viz.

$$\bar{r}=\frac{r}{a}=S(\tau,\eta)e^{\pi\xi} \tag{10}$$

## Notation

| | |
|---|---|
| $a$ | Radius of cylinder |
| $c$ | Specific heat |
| $D$ | Diameter of cylinder |
| Fo | Fourier number, $\alpha t/a^2$ |
| $g$ | Transformed coefficient |
| $h$ | Heat transfer coefficient |
| $k$ | Thermal conductivity |
| $L$ | Latent heat |
| Nu | Nusselt number, $hD/k$ |
| $\mathrm{Nu}_e$ | Effective Nusselt number, $h(\bar{S}D)/k$ |
| Pr | Prandtl number, $\nu/\alpha$ |
| $q$ | Surface heat transfer rate |
| $r$ | Radial coordinate |
| $\bar{r}$ | Dimensionless radial coordinate, $r/a$ |
| $R$ | Phase change location |
| Re | Reynolds number, $UD/\nu$ |
| $\mathrm{Re}_e$ | Effective Reynolds number, $U(\bar{S}D)/\nu$ |
| $R_{\mathrm{th}}$ | Thermal resistance |
| $S$ | Dimensionless phase change location, $R/a$ |
| $\bar{S}$ | Average dimensionless phase change location |
| Ste | Stefan number, $c_s(T_f-T_w)/L$ |
| $t$ | Time |
| $\tilde{T}$ | Temperature |
| $T$ | Dimensionless temperature, $(\tilde{T}-\tilde{T}_w)/(\tilde{T}_f-\tilde{T}_w)$ |
| $\tilde{u},\tilde{v}$ | Velocity components in $\theta$- and $r$-direction |
| $U$ | Velocity at infinity |
| $V/V_0$ | Ratio of ice deposition volume to cylinder volume, $\bar{S}^2-1$ |

*Greek symbols*

| | |
|---|---|
| $\alpha$ | Thermal diffusivity |
| $\zeta$ | Transformed $r$-coordinate (solid region) |
| $\eta$ | Transformed $\theta$-coordinate |
| $\theta$ | Angular coordinate |
| $\lambda$ | Parameter for fluid superheat or subcooled cylinder, $(\tilde{T}_0-\tilde{T}_f)/(\tilde{T}_f-\tilde{T}_w)$ |
| $\nu$ | Kinematic viscosity |
| $\xi$ | Transformed $r$-coordinate (liquid region) |
| $\tau$ | Dimensionless time, $Ut/a$ |
| $\tilde{\psi}$ | Stream function |
| $\psi$ | Dimensionless stream function, $\tilde{\psi}/Ua$ |
| $\tilde{\omega}$ | Vorticity |
| $\omega$ | Dimensionless vorticity, $\tilde{\omega}a/U$ |

*Subscripts*

| | |
|---|---|
| av | Average value |
| $f$ | Frozen state, fusion |
| $l$ | Liquid material |
| max | Maximum value |
| 0 | Initial condition or outer boundary |
| $s$ | Solid material |
| s.p. | Stagnation point |
| sep | Flow separation |
| $w$ | Cylinder wall |

and

$$\theta=\pi\eta \tag{11}$$

where

$$S(\tau,\eta)=R/a \quad \text{and} \quad \tau=Ut/a \tag{12a,b}$$

are the dimensionless interface location and the convective time, respectively.

Nondimensionalization of Equations 1, 2, and 5 yields

$$g(S,\xi)\left(\frac{\partial\omega}{\partial\tau}-\frac{1}{\pi S}\frac{\partial S}{\partial\tau}\frac{\partial\omega}{\partial\xi}\right)+\left(\frac{\partial\psi}{\partial\xi}\frac{\partial\omega}{\partial\eta}-\frac{\partial\psi}{\partial\eta}\frac{\partial\omega}{\partial\xi}\right)=\frac{2}{\mathrm{Re}}\nabla^2\omega \tag{13}$$

$$-\nabla^2\psi=\omega \tag{14}$$

and

$$g(S,\xi)\left(\frac{\partial T}{\partial\tau}-\frac{1}{\pi S}\frac{\partial S}{\partial\tau}\frac{\partial T}{\partial\xi}\right)+\left(\frac{\partial\psi}{\partial\xi}\frac{\partial T}{\partial\eta}-\frac{\partial\psi}{\partial\eta}\frac{\partial T}{\partial\xi}\right)=\frac{2}{\mathrm{Re\,Pr}}\nabla^2T \tag{15}$$

where

$$g(S,\xi)=\pi^2S^2e^{2\pi\xi} \tag{16a}$$

and

$$\nabla^2=\left(1+\left(\frac{1}{\pi S}\frac{\partial S}{\partial\eta}\right)^2\right)\frac{\partial^2}{\partial\xi^2}-\frac{2}{\pi S}\left(\frac{\partial S}{\partial\eta}\right)\frac{\partial^2}{\partial\xi\,\partial\eta}+\frac{\partial^2}{\partial\eta^2}+\frac{1}{\pi S}\left(\frac{1}{S}\left(\frac{\partial S}{\partial\eta}\right)^2-\frac{\partial^2S}{\partial\eta^2}\right)\frac{\partial}{\partial\xi} \tag{16b}$$

The boundary conditions 4 and 6 become

$$\psi=\frac{\partial\psi}{\partial\xi}=0 \quad \text{and} \quad -\nabla^2\psi|_{r=R}=\omega \qquad \text{for } r=R$$

$$\omega=0 \quad \text{and} \quad \psi=2\cosh(\pi\xi)\sin(\pi\eta) \qquad \text{at infinity}$$

$$\tau\geq\tau_0: \qquad \psi=\omega=0 \qquad \text{on } \eta=0,1 \tag{17}$$

and

$$\tau<\tau_0: \qquad T=T_0$$

$$\tau\geq\tau_0: \qquad T=1 \qquad \text{for } \xi=0$$

$$T=T_0 \qquad \text{at infinity}$$

$$\frac{\partial T}{\partial\eta}=0 \qquad \text{on } \eta=0,1 \tag{18}$$

For the *solid* region, the transformations reported by Ho and Chen[2] have been used

$$\zeta=\frac{\bar{r}-1}{S(\mathrm{Fo},\eta)-1} \quad \text{and} \quad \theta=\pi\eta \tag{19a,b}$$

While $S(\mathrm{Fo},\eta)$ stays the same, a new (diffusive) time for the solid region, the Fourier number, is introduced

$$\mathrm{Fo}=\frac{\alpha t}{a^2}=\frac{2}{\mathrm{Re\,Pr}}\left(\frac{\alpha_s}{\alpha_l}\right)\tau \tag{19c}$$

Equation 7 now reads

$$\frac{\partial T}{\partial\mathrm{Fo}}-\frac{\zeta}{S-1}\frac{\partial S}{\partial\mathrm{Fo}}\frac{\partial T}{\partial\zeta}=\nabla^2T \tag{20}$$

where

$$\nabla^2=\left[\left(\frac{1}{S-1}\right)^2+\frac{1}{\pi^2\bar{r}^2}\left(\frac{\zeta}{S-1}\right)^2\left(\frac{\partial S}{\partial\eta}\right)^2\right]\frac{\partial^2}{\partial\zeta^2}-\frac{2}{\pi^2\bar{r}^2}\frac{\zeta}{S-1}\frac{\partial S}{\partial\eta}\frac{\partial^2}{\partial\zeta\,\partial\eta}+\frac{2}{\pi^2\bar{r}^2}\frac{\partial^2}{\partial\eta^2}+\frac{1}{\bar{r}(S-1)}\left[1+\frac{\zeta}{\pi^2\bar{r}}\left(\frac{2}{S-1}\left(\frac{\partial S}{\partial\eta}\right)^2-\frac{\partial^2S}{\partial\eta^2}\right)\right]\frac{\partial}{\partial\zeta} \tag{21}$$

The nondimensional energy balance for the liquid–solid interface becomes

$$\frac{\partial S}{\partial\mathrm{Fo}}=\mathrm{Ste}\left[1+\left(\frac{1}{\pi S}\frac{\partial S}{\partial\eta}\right)^2\right]\left(\frac{1}{S-1}\frac{\partial T}{\partial\zeta}-\frac{k_l}{k_s}\frac{1}{\pi S}\frac{\partial T}{\partial\xi}\right) \tag{22}$$

Defining an effective Nusselt number as

$$\mathrm{Nu}_e=\frac{h\bar{S}D}{k} \tag{23a}$$

which reflects heat transfer at the moving boundary location, the local heat transfer coefficient can now be computed from

$$\mathrm{Nu}_e=\frac{2}{\pi}\frac{\partial T/\partial\xi}{\lambda} \tag{23b}$$

## Numerical solution method

Using the previously described coordinate transformations, the solid region is mapped onto a $1\times1$ square domain which is discretized using a $51\times21$ grid where $\Delta\eta=1/50$ and $\Delta\zeta=1/20$. The liquid region, bounded by a radius of $\xi=1$ which corresponds to about 23 times of the cylinder radius, also forms a square domain with $\Delta\eta=1/50$ and $\Delta\xi=1/40$ or $\Delta\xi=1/30$ depending upon the Reynolds number. An alternate direction implicit finite difference code has been developed to solve Equations 13–15, 20, and 22 subject to the boundary conditions 17 and 18. An upwind difference scheme is applied for the convective terms in Equation 15. In general, central differencing is used for the spatial derivatives whereas time derivatives are approximated by a forward difference operator. As an initial condition, a thin ice layer on the cylinder surface is assumed to get the numerical computation started. The thickness of this initial layer depends on the Stefan number and the superheat of the fluid. Prusa and Yao[1] pointed out that the effect of the incorrect initial interface decays very rapidly. It was found that setting $S=1.05$ initially resulted in stable and accurate numerical solutions. The location of the moving boundary is calculated from the temperature distributions of the liquid and solid regions at the end of each time step. Using small time steps ($\Delta\tau<0.05$), the discontinuity caused by the moving solidification front is negligible for low Stefan number problems; hence intermediate iterations are not necessary. Results from repeat calculations with finer grids indicated that mesh-independence has been achieved.

## Results and discussion

The predictive capabilities of the new model have been tested by comparing numerical results with experimental data sets from releated case studies. Then, the validated computer simulation model has been used to analyze flow patterns, isotherms, and ice layer formations for different system parameters.

### *Comparison with published data*

In Table 1, characteristic parameters for single-phase, thermal flow past a horizontal cylinder have been summarized. The comparison between predicted and measured data is very good

**Table 1** Data comparison for single-phase thermal cross flow past a cylinder ($\theta_{sep}$ is measured counterclockwise)

| | Separation angle $\theta_{sep}$ | | Drag coefficient $C_D$ | | Nusselt numbers (Pr=1.0) $Nu_{s.p.}$ | | $Nu_{av}$ | |
|---|---|---|---|---|---|---|---|---|
| $Re_d$ | Model | [Ref. 10] | Model | [Ref. 11] | Model | [Ref. 9] | Model | [Ref. 12] |
| 10 | 30° | 32° | 2.92 | 2.85 | — | — | — | — |
| 20 | — | — | — | — | 12.5 | 12.9 | 7.1 | 6.5 |
| 40 | 54.6° | 54.5° | 1.52 | 1.52 | — | — | — | — |
| 50 | — | — | — | — | 16.4 | 17.1 | 10.7 | 10.3 |
| 70 | 62.5° | 62.5° | 1.22 | 1.21 | — | — | — | — |
| 100 | 67.7° | 67.7° | 1.08 | 1.06 | 22.2 | 24.2 | 14.5 | 14.5 |

except for higher Reynolds numbers (Re > 100) when vortex shedding may influence $\theta_{sep}$, $C_D$, and Nu-values.

Conduction-dominated ice formation around circular cylinders (Re = 0) has been analyzed by Lunardini.[6] Figure 2 shows a comparison of the transient interface location for freezing water between Lunardini's results and our model predictions.

### *Flow patterns and isotherms*

Ice layer growth as well as the temporal development of streamlines and isotherms are shown in a sequence of graphs (Figures 3(a)–(c)) for typical values of the key parameters. The results confirm the assumption of concentric ice layer growth in the beginning stage. While the free stream velocity stays constant, the local Reynolds number increases as the solid–liquid interface moves outwards with time, $1 \leq Fo \leq 7$. Thus, the recirculation zone expands which in turn affects the overall heat transfer process. The isotherms are quite evenly spaced along the front part of the cylinder, $0° \leq \theta \leq 50°$, and near the rear stagnation point, i.e., $160° < \theta \leq 180°$. As a result, the local heat transfer coefficient and, in turn, the ice layer thickness should be rather uniform within these two angular sections (cf. Figures 4(b) and 5).

### *Ice layer formation*

Conduction heat transfer in the solid region plays an important role during the freezing process. Because of the very steep temperature gradients across the initially thin ice layer, large amounts of heat are withdrawn from the adjacent liquid. Figure 4(a) shows the transient interfacial heat flux ratio for different Reynolds numbers, where

$$\frac{q_s''}{q_l''} = 1 + \frac{k_s/k_l}{\lambda \, Nu_e \, Ste} \frac{\partial \bar{S}^2}{\partial Fo} \tag{24}$$

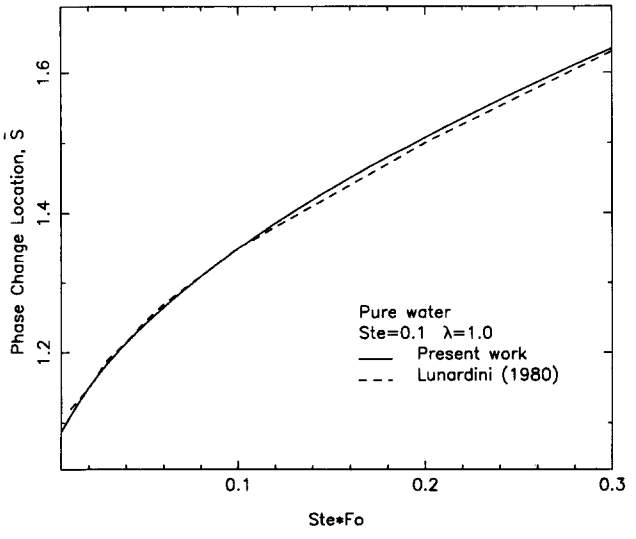


*Figure 2* Data comparison of transient solid–liquid interface location for conduction controlled process

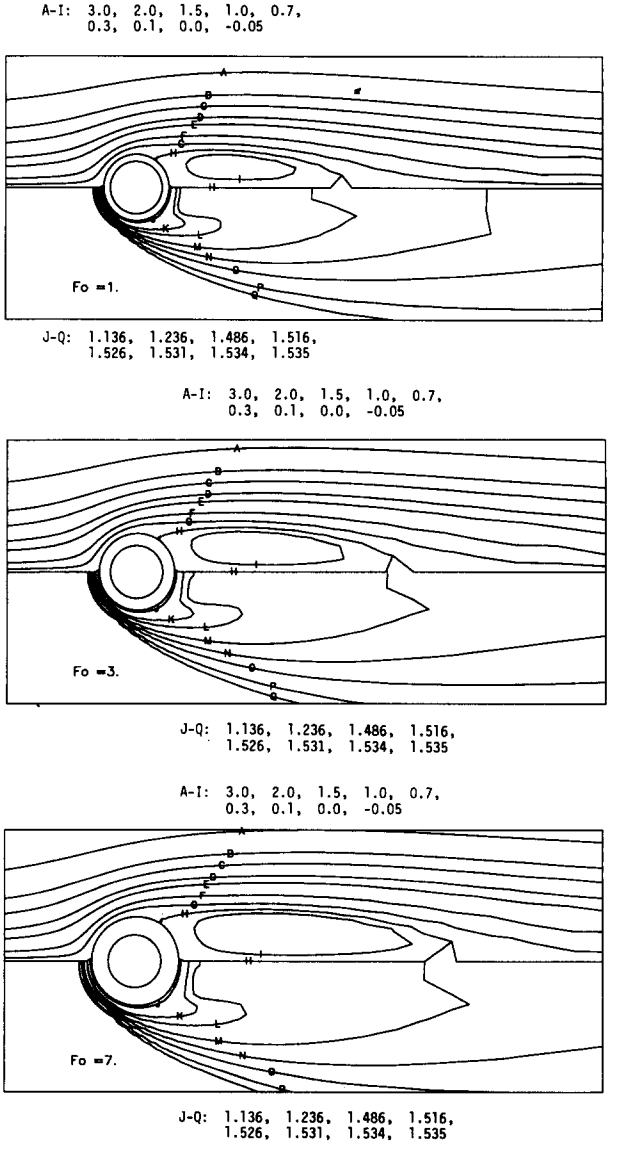


*Figure 3* Streamlines, isotherms and ice formation around cylinder at three time levels Fo = 1, 3 and 7 (Re = 50, Pr = 13, Ste = 0.03616 and $\lambda = 0.5395$)

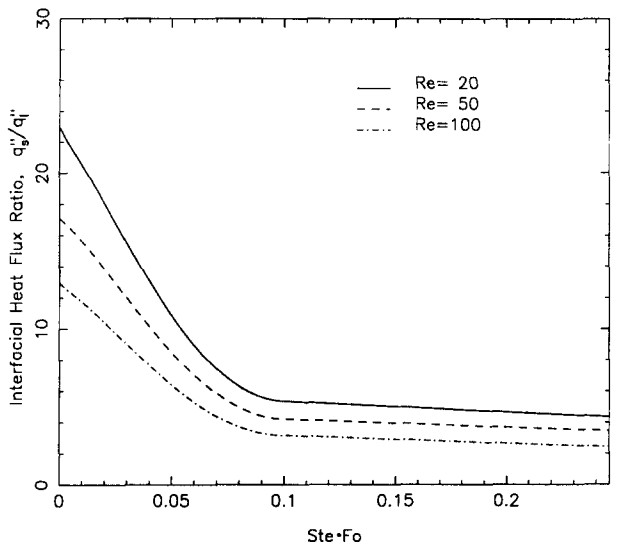


*Figure 4(a)* Transient heat flux ratio at the solid–liquid interface for different free-stream Reynolds numbers (Ste = 0.3615, $\lambda = 0.5395$)

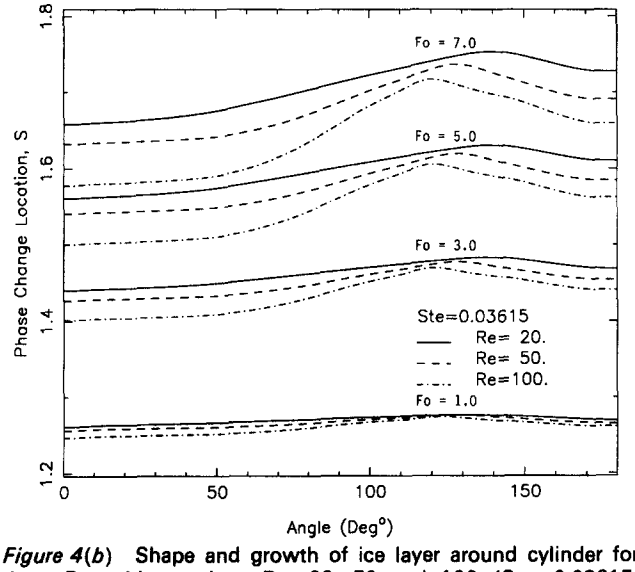


*Figure 4(b)* Shape and growth of ice layer around cylinder for three Reynolds numbers Re = 20, 50 and 100 (Ste = 0.03615, $\lambda = 0.5395$ and Pr = 13.0)

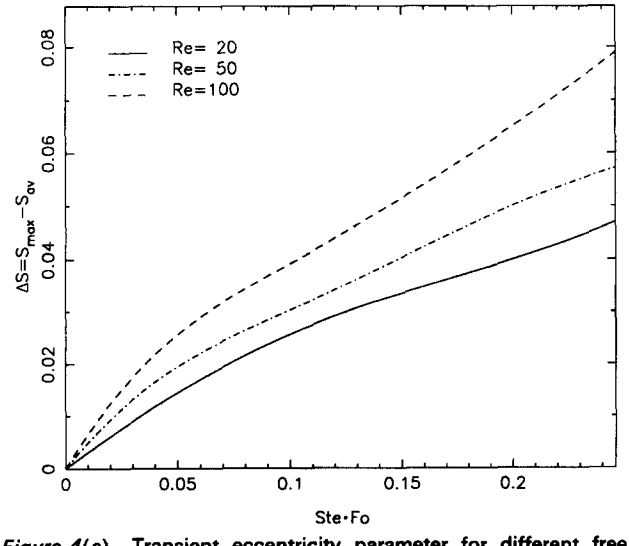


*Figure 4(c)* Transient eccentricity parameter for different free-stream Reynolds numbers (Ste = 0.03615, $\lambda = 0.5395$)

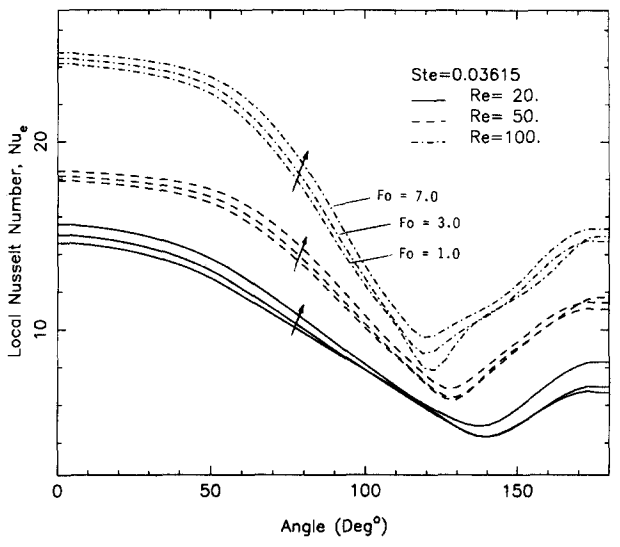


*Figure 5* Local Nusselt number distribution at three time levels Fo = 1, 3 and 7 for Re = 20, 50 and 100 (Ste = 0.03615, $\lambda = 0.5395$ and Pr = 13.0)

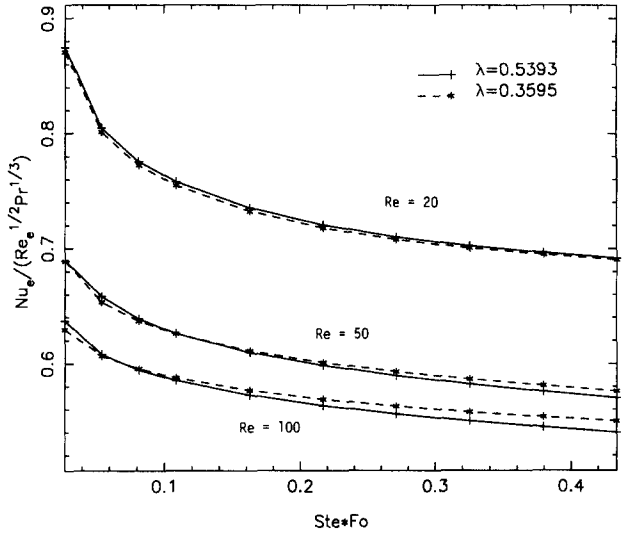


*Figure 6* Average Nusselt number profiles as a function of Stefan number and Fourier number for different free-stream Reynolds numbers and superheat parameters

In the early stages, the concentric ice build-up is almost entirely controlled by the thermal diffusion and latent heat balance. After some time (i.e., Ste Fo > 0.1), when the thermal resistance of the growing ice layer, $R_{th} \sim \ln(R/a)$, increases, the influence of variations in convection heat transfer becomes significant (i.e., Fo > 1) and the ice layer thickness varies with location and Reynolds number (Figure 4(b)). Such a dependence of $S = S(\theta, \mathrm{Re})$ is even more dramatic when the fluid is superheated or the cylinder is subcooled, i.e., when $\lambda$ increases. Figure 4(c) indicates the increase of "eccentricity" in ice formation around a cylinder with dimensionless time. Here, $S_{max}$ is the maximum dimensionless interface location (cf. Figure 4(b)) and $S_{av} = \bar{S}$ is the average dimensionless radius for the cylinder plus ice layer configuration.

The temporal changes of the local Nusselt number (cf Equation 23b) for different free stream Reynolds numbers are shown in Figure 5. The graphs $Nu_e(\theta)$ reflect the isotherm patterns along the cylinder wall as discussed in conjunction

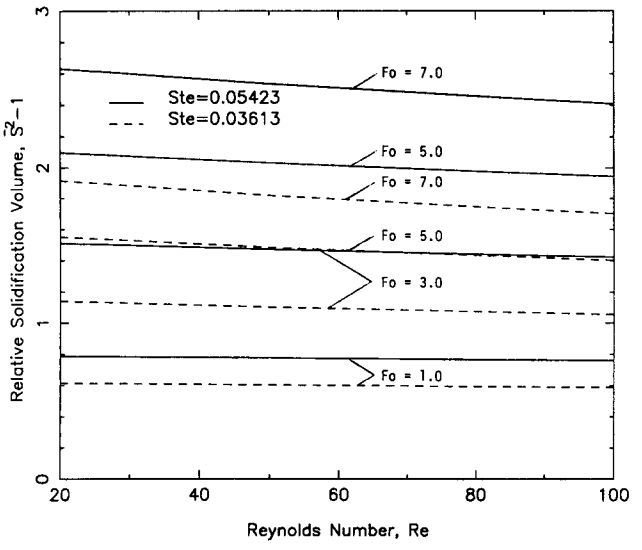


*Figure 7* Relative solidification volume as a function of Reynolds number for different Stefan numbers and Fourier numbers

with Figure 3. After flow separation, the heat transfer coefficient has a minimum because the recirculating fluid attains radially a rather uniform temperature; as a result, $Nu_e \sim \partial T/\partial \xi$ is small.

Figure 6 depicts the average Nusselt number at the interface as a function of dimensionless time, Ste·Fo, for different Reynolds numbers and for two superheat values. For a given Stefan number, it is evident that the amount of heat transferred and hence the effective Nusselt number is initially large and then levels off swiftly, especially at low Reynolds numbers.

Figure 7 indicates that decreasing the Stefan number, i.e., maintaining higher cylinder wall temperatures will retard the solidification rate. Ice production is almost independent of the Reynolds number at low Fourier numbers ($Fo \leq 1.0$), when the phase change process is heat conduction controlled, i.e., $Ste \cdot Fo \ll 1$.

## Conclusions

The unsteady Navier–Stokes equation in the stream function–vorticity formulation and the energy equation have been solved for laminar two-dimensional flow past a subcooled cylinder with outward solidification. Suitable coordinate transformations allowed mapping of the irregular, moving solid–liquid regions into uniform squares for easier numerical solution using an ADI finite difference scheme. The validated computer simulation model has been used to study transient thermal flow patterns, interface locations, Nusselt number distributions and rates of ice formation for different Reynolds numbers, superheat parameters and Stefan numbers.

Forced convection heat transfer may have a strong effect on the freezing process. Although initially heat conduction controlled, the rate of ice layer growth is retarded at high Reynolds numbers flows. At low Stefan numbers or high superheat parameters, the shape of ice formation can be very irregular, invalidating the commonly employed assumption of uniform ice layer growth.

## References

1 Prusa, J. and Yao, L. S. Melting around a horizontal heated cylinder: Part II—Numerical solution for isothermal boundary condition. *Int. J. Heat Mass Transfer* 1984, **106**, 467–472

2 Ho, C. J. and Chen, S. Numerical simulation of melting of ice around a horizontal cylinder. *Int. J. Heat Mass Transfer* 1986, **29**, 1359–1369

3 Hirata, T., Gilpin, R. R., Cheng, K. C., and Gates, E. M. The steady-state ice layer profile on a constant temperature plate in a laminar forced convection flow. *Int. J. Heat Mass Transfer* 1979, **22**, 1425–1433

4 Lock, G. S. H. and Kaiser, T. M. V. Icing on submerged tubes: a study of occlusion. *Int. J. Heat Mass Transfer* 1985, **28**, 1689–1698

5 Karniadakis, G. E. Numerical simulation of forced convection heat transfer from a cylinder in crossflow. *Int. J. Heat Mass Transfer* 1988, **31**, 107–118

6 Lunardini, V. J. Phase change around a circular cylinder. ASME Winter Annual Mtg., Nov. 1980, Chicago, IL, Paper 80-WA/HT-5, ASME, N.Y., N.Y., 1980

7 Solomon, A. D., Alexiades, V., Wilson, D. G., and Drake, J. The formulation of a hyperbolic Stefan problem, Tedin. Report ORNL-6065, Oak Ridge Nat'l Lab, Oak Ridge, TN, Oct. 1984

8 Anderson, D. A., Tannehill, J. C., and Pletcher, R. H. *Computational Fluid Mechanics and Heat Transfer*, McGraw-Hill, 1984

9 Okada, M., Katayama, K., and Terasaki, K. Freezing around a cooled pipe in crossflow. *Bulletin of the JSME* 1978, **21**, 160–172

10 Grove, A. S., Shair, F. H., and Acrivos, A., An experimental investigation of the steady separated flow past a circular cylinder. *J. Fluid Mech.* **19**, 60–80, 1964

11 Dennis, S. C. R. and Chang, Gau-Zu, Numerical solutions for steady flow past a cylinder at Reynolds number up to 100. *J. Fluid Mech.* 1970, **42**, 471–489

12 Eckert, E. R. G. and Drake, R. M. *Analysis of Heat and Mass Transfer*, McGraw-Hill, New York, 1972